ISSN 1054-660X, Laser Physics, 2009, Vol. 19, No. 2, pp. 336–341.

Filament-Induced Birefringence in Argon[1]

Y. Petit[a], *, P. Béjot[a], L. Bonacina[a], J. Kasparian[b], M. Moret[a], and J.-P. Wolf[a]

[a] *GAP, Université de Genève, 20 rue de l'Ecole de Médecine, CH-1211 Genève 4, Switzerland*

[b] *Teramobile, Université Lyon 1; CNRS; LASIM UMR 5579, bât. A. Kastler, 43 Bd du 11 novembre 1918, F-69622 Villeurbanne Cedex, France*

*e-mail: Yannick.petit@unige.ch

Received September 30, 2008

Abstract—We demonstrate that a driving ultrashort laser pulse undergoing filamentation can induce a remarkably large birefringence in Argon, resulting in an ultrafast "half-wave plate" for a copropagating non-filamenting probe beam. Such femtosecond birefringence, which originates from the difference between the nonlinear refractive indices induced by the filament on the axes parallel and orthogonal to its own polarization, opens the way to potential ultrafast Kerr-gates whose ultimate time-duration is only restricted by the duration of the driving pulse. We also show that the induced birefringence is transversely inhomogeneous, resulting from to the intensity profile of the driving pulse.

PACS numbers: 42.65.Re, 42.65.Sf, 42.65.Jx

DOI: 10.1134/S1054660X09020273

1. INTRODUCTION

The propagation of laser beams undergoing filamentation in gases is now a well understood process, resulting from a dynamical balance between Kerr self-focusing and defocusing on laser-generated plasma [1–5]. Detailed characterizations have been performed on the spectral, temporal and spatial behavior of filaments. These light structures provide unique capabilities for applications like atmospheric remote sensing [6], lightning control [5, 7], few-cycle pulses generation [8–10], as they can deliver high intensities (several 10^{13} W/cm^2) over distances far beyond the usual diffraction limit.

Up to now, polarization has been somehow left apart in investigations to date. A few pioneering works studied the influence of the incident polarization on the filament themselves [11–14]. Filament-induced changes in the refractive index of air have only been considered for long-lasting effects (nanoseconds to microseconds) of the plasma left behind the pulse [15, 16]. Even if self-induced birefringence has been observed to generate refractive index changes Δn in the 10^{-5} range for ultrashort lasers focused into gases [17], the resulting phase shift remains marginal as diffraction restricts the effect to a Rayleigh length of about 100 μm around the beam waist position.

In this paper, we demonstrate that the unique interaction length and the high-intensity conveyed by laser filaments in a rare gas, Argon here, can induce a "half-wave plate" effect, providing the ability to rotate the incident linear polarization of a non-filamenting probe pulse by an arbitrarily chosen angle. We also show that the transverse intensity distribution of the filamenting beam leads to an inhomogeneous birefringence across the probe beam profile. Consequently, the femtosecond birefringence profile presents an inhomogeneous transverse distribution within the probe profile. Such consideration could be an appropriate method for non-destructive measurement of the distribution of the longitudinally-integrated intensity profile of the filament.

2. EXPERIMENTAL SETUP

The experimental setup has been described in detail in [18] (Fig. 1). A Ti:Sa amplifier system associated with a delay line and a BBO doubling crystal delivers two slightly chirped pulses, respectively red (800 nm, 1 mJ, 100 fs) and blue (400 nm, 1 μJ, 100 fs), with a tunable time delay. The red pulse polarization is rotated by a zero-order waveplate (WP), and its orientation is taken as reference (x axis, $\theta = 0°$). The two beams are slightly focused by a 1 m focal lens in a 2 m long cell filled with tunable pressure Argon.

The driving (red) pulse generates a single filament, whereas the probe (blue) pulse propagates linearly in absence of the driving pulse. We measured the time-integrated probe intensity of each pulse as a function of the output polarizer orientation, for chosen positions in the beam profile. Using this technique, a linear polarization appears as a squared cosine function, as described in Figs. 2a and 2b. We used a 0.5 nm resolution monochromator to discriminate between the two pulses.

We also compared the experimental results with numerical simulations based on a 2D + 1 model, as described in detail before [18–20]. We considered pump input parameters corresponding to our experiment (i.e., an energy $E = 750$ μJ, a Fourier-limited pulse duration $\Delta t_{\mathrm{FWHM}} = 30$ fs, and a residual chirp of

[1] The article is published in the original.

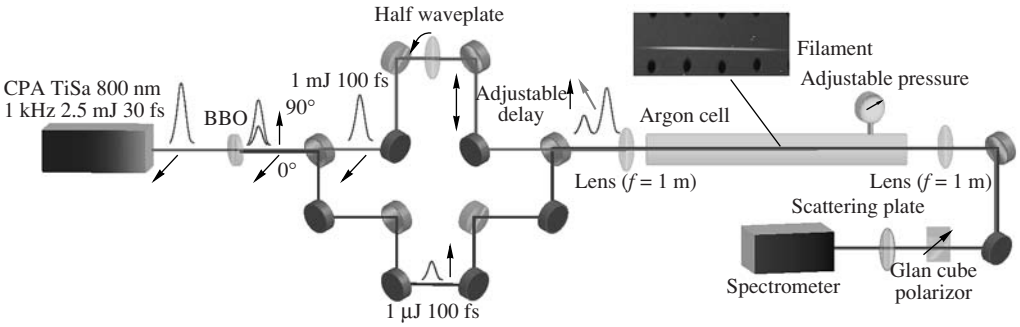

Fig. 1. Experimental setup. DCM: Dichroic mirror. HWP: half-wave plate. The linear polarization of the red pulse (800 nm) is set relative to that of the blue pulse (400 nm) before their interaction in the Argon cell. These copropagating beams are separated by a spectrometer their polarization is analyzed by rotating a Glan cube. Diaphragm is shortly open for the experiments described in Sections 3 and 5, and fully open for Section 6 [18].

330 fs^2), and we calculated the evolution of the pump pulse intensity profile as a function of propagation distance z for each considered Argon pressure.

3. FILAMENT-INDUCED ULTRAFAST HALF-WAVE PLATE

Figure 2 illustrates the experimentally measured modification of the probe beam polarization at the exit of the cell (filled with a 3 bar Argon pressure) when its initial polarization is set at $\alpha_{input} = -55°$ with respect to the driving beam polarization and the two pulses temporally overlap. After the interaction, the probe beam polarization remains highly linear with a contrast ratio $(I_{max}^{probe} - I_{min}^{probe})/(I_{max}^{probe} + I_{min}^{probe})$ as high as 98.4%, but rotated to $\alpha_{output} = 57 \pm 2°$, symmetrical to the initial one with regard to that of the filamenting pump beam. This probe polarization flipping is the same as would be obtained with a half-wave plate inserted in the probe beam path with its neutral axis at 0°. More precisely, the observed filament-induced birefringence corresponds to a $\lambda_{probe}/2.1$ "waveplate," i.e., the difference in the optical paths between the parallel and the perpendicular components of the probe beam amounts 1/2.1 optical cycle at 400 nm. Such a remarkably large dephasing provides a way to tilt the linear polarization of an ultrashort laser pulse by a controlled amount: the angle of rotation of the probe polarization is twice the angle that is initially set between the input probe pulse polarization and the filamenting pump pulse polarization. In particular, choosing a 45° angle between the polarizations of the driving and probe beams flips the probe polarization by 90° at the cell exit. Setting the polarizer perpendicular to the initial probe polarization allows then to switch the probe beam intensity on and off by switching the driving pulse on and off.

As shown in Fig. 3, this polarization switching critically depends on the time delay between the two pulses (200 fs), corresponding to the measured cross-correlation between the pump undergoing filamentation and the probe beam. Moreover, the birefringence dependence with the delay is symmetric with respect to time reversal, which is consistent with the fact that the optical Kerr effect in a monoatomic rare gas like Argon is instantaneous. The duration of the observed "filament-induced Kerr gate" is thus fully controlled by that of the driving laser pulse. Using few-cycle pulses as driving lasers could therefore lead to optical gates with unprecedented time resolution (Fig. 4). Such gates could convert information encoded in the temporal intensity profile of the driving pulse into the temporal polarization profile of the probe beam [21].

4. THEORETICAL DESCRIPTION

The mechanism of the observed filament-induced birefringence can be explained by the difference in the nonlinear refractive indices generated by the driving laser pulse along its polarization axis and the orthogo-

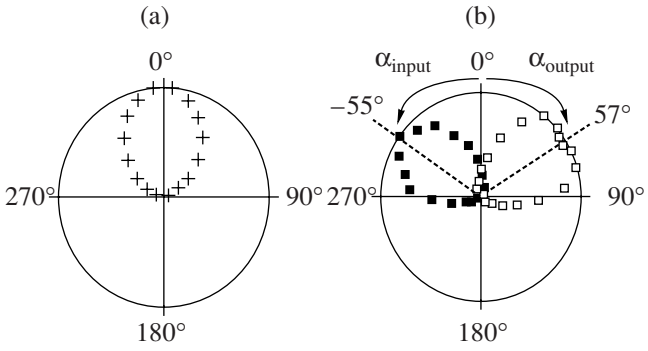

Fig. 2. Polar plot of the intensity transmitted as a function of the analyzing polarizer angle, for a 3 bar Argon pressure. For clarity, only half of the pattern is shown, the other half being given by symmetry. (a) Driving pulse (filament) polarization set at 0°. (b) Input (blue, $\alpha_{input} = -55°$) and output (green, $\alpha_{output} = 57°$) polarizations of the probe pulse. Co-propagation with the filament flips the probe polarization to an axis symmetrically around the driving pulse polarization. The squared *cosine* patterns are signatures for linearly polarized light [18].

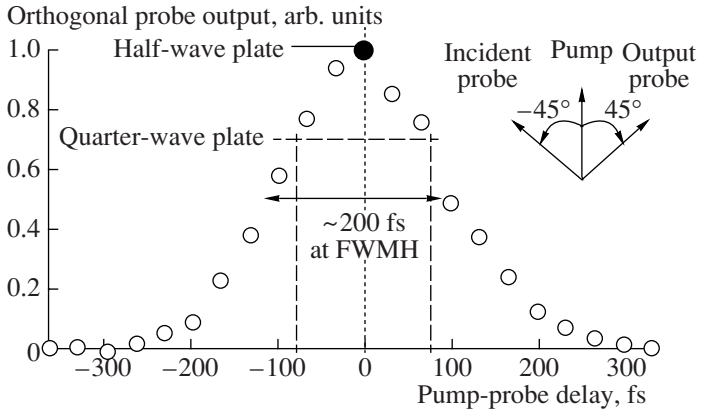

Fig. 3. Output probe intensity measured with a polarizer orthogonal to the probe beam input polarization, as a function of the pump-probe delay. Here, a pump polarization at 45° and a 3 bar Argon pressure of 3 bar are considered [21]. Possibility to perform quarter-wave plate for ±80 fs delays, as the transmission of the orthogonal probe output is $\sqrt{2}/2$.

nal axis, respectively. More precisely, the driving field E^{filament}, polarized along the x-axis (therefore implying $E_y^{\text{filament}} = 0$), induces a symmetry breaking in the optical response of the isotropic Argon gas. The nonlinear Kerr polarizations of the probe beam along x and y respectively read [22]:

$$P_{\text{XMP},\,x}^{\text{probe}} = \frac{3\varepsilon_0}{2}\chi_{xxxx}^{(3)}\left|E_x^{\text{filament}}\right|^2 E_x^{\text{probe}}, \qquad (1)$$

$$P_{\text{XMP},\,y}^{\text{probe}} = \frac{3\varepsilon_0}{2}\chi_{yyxx}^{(3)}\left|E_x^{\text{filament}}\right|^2 E_y^{\text{probe}}, \qquad (2)$$

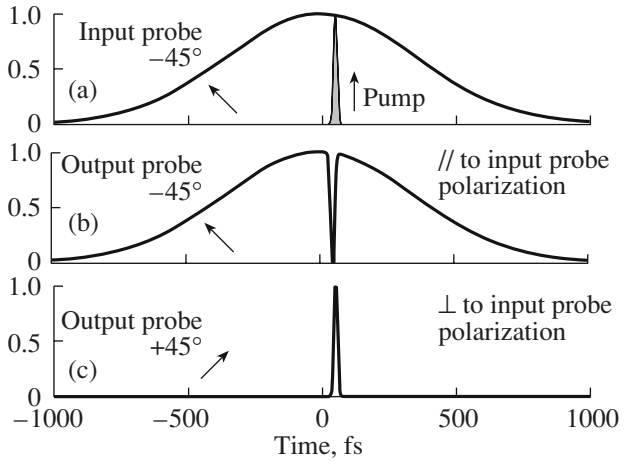

Fig. 4. Principle of an ultrafast Kerr-gate based on a filamenting pump beam. (a) Long probe beam and ultrashort pump beam, with linear polarizations at 45° from each other. (b, c) Output probe intensity, respectively parallel and orthogonal to the incident probe polarization [21].

where XPM stands for the probe Cross-Phase Modulation induced by the filamenting pulse, and the nonlinear elements $\chi_{ijkl}^{(3)} = \chi_{ijkl}^{(3)}(\lambda_{\text{probe}};\, \lambda_{\text{probe}},\, \lambda_{\text{pump}},\, -\lambda_{\text{pump}})$ are related to the considered cross-Kerr process. All the other nonlinear Kerr polarization terms are negligible here, as the ratio of the probe and driving beam energies is 10^{-3}. The dominant contribution to the $\chi^{(3)}$ tensor in atomic rare gases, like Argon, is governed by the electronic cloud response (i.e., by the atomic nonlinear polarizability). The plasma contribution to $\chi^{(3)}$ is neglected because of the relatively low concentration of ions with respect to neutral molecules (typically 10^{-4} [23]), and because free electrons only have a significant contribution in the relativistic regime [24]. Since the filament and probe frequencies are far from any resonant transition in the case of Argon, we can consider that $\chi_{xxxx}^{(3)} = 3\chi_{yyxx}^{(3)}$ [22]. As a consequence, the filament-induced birefringence is:

$$\Delta n_{\text{XPM}}^{\text{probe}} = \frac{1}{2n_0}\left(\frac{3}{2}\text{Re}(\chi_{xxxx}^{(3)} - \chi_{xxyy}^{(3)})\right)\left|E_x^{\text{filament}}\right|^2 = n_2^{\text{XPM}} I^{\text{filament}} \qquad (3)$$

with

$$n_2^{\text{XPM}} = \text{Re}(\chi_{xxxx}^{(3)})/(n_0^2\varepsilon_0 c) = 4n_2/3\,. \qquad (4)$$

Here, n_2^{XPM} is the XPM nonlinear refractive index of Argon, I^{filament} the intensity within the filament, $n_0 = 1.0003$ the linear refractive index of Argon at the probe frequency for experimental pressures at room temperature, ε_0 the vacuum permittivity and c the speed of light in vacuum, n_2 is the "usual" nonlinear refractive index as defined, e.g., in [2–5]. Integrated over the whole interaction length, this birefringence induces a dephas-

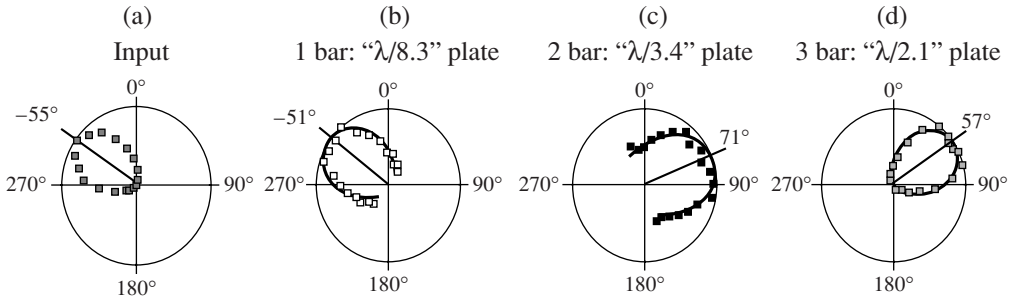

Fig. 5. Pressure dependence of the filament-induced birefringence. (a) Input probe polarization; (b–d) Output probe beam polarization for 1, 2, and 3 bar respectively. The black solid lines are fits assuming elliptical polarizations [18].

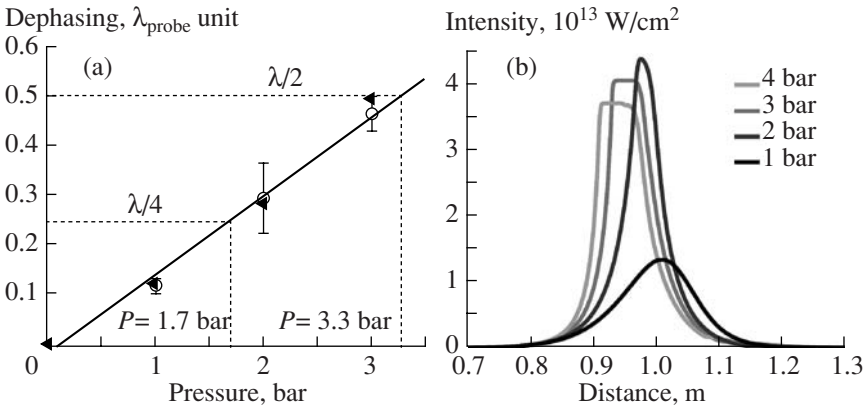

Fig. 6. (a) Experimental (circles) and simulated (triangular) pressure dependence of the filament-induced dephasing. (b) Evolution of the intensity at the filament center with the propagation distance, depending on the pressure [18].

ing between the probe beam components along the fast and slow polarization axes of:

$$\Delta\varphi_{\mathrm{XPM}}^{\mathrm{probe}} = 2\pi\int\Delta n_{\mathrm{XPM}}^{\mathrm{probe}}dz/\lambda_{\mathrm{probe}} = 2\pi n_2^{\mathrm{XPM}}\int I^{\mathrm{filament}}(z)dz/\lambda_{\mathrm{probe}}. \quad (5)$$

5. PRESSURE DEPENDENCE OF INDUCED BIREFRINGENCE

The filamented-induced dephasing $\Delta\varphi_{\mathrm{XPM}}^{\mathrm{probe}}$ varies with the nonlinear refractive index n_2^{XPM}, and hence, with the Argon pressure in the cell at a fixed temperature at 21°. The measured birefringence at different Argon pressures is presented in Fig. 5. A pressure close to 3 bar (precisely 3.3 ± 0.2 bar) permits to generate an ideal half-wave plate. For lower pressures, an elliptical polarization is observed. A fit of the angular pattern of the output polarization (Figs. 5b–5d) yields a contrast ratio of 67.7% at 1 bar, 39.5% at 2 bar and 98.4% at 3 bar, as well as the orientation of their ellipticity main axis, which amounts to $\alpha_{\mathrm{output}} = -51° \pm 3°$, $71° \pm 5°$, and $57° \pm 2°$, respectively. This elliptical polarization is the signature for a smaller dephasing $\Delta\varphi_{\mathrm{XPM}}^{\mathrm{probe}}$, corresponding to $\lambda_{\mathrm{probe}}/8.3$ at 1 bar and $\lambda_{\mathrm{probe}}/3.4$ at 2 bar, respectively, Fig. 5a.

To gain more insight into the pressure dependence, we compared the experimental results with the output of the numerical simulations providing the longitudinal intensity profile at the different pressures, and thus the corresponding birefringence $\Delta n_{\mathrm{XPM}}^{\mathrm{probe}}$ through Eq. (3). This dephasing depends linearly on the Argon pressure, in excellent agreement with the experimental data (Fig. 6a) for a value of n_2^{XPM} proportional to the Argon pressure and equal to 1.6×10^{-20} cm^2/W at 1 atm. This value lies below that expected from Eq. (4). Such underestimation is due to the fact that the calculations overestimate the pump intensity, because simulations consider that of the beam center while the actual measurement is integrated over 1 mm diameter. Moreover, the temporal walk-off of both pulses due to group-velocity dispersion in Argon is not taken into account in our calculations. Further work is required to provide quantitative transverse and temporal profiles of filament-induced birefringence, and achieve a better quantitative agreement.

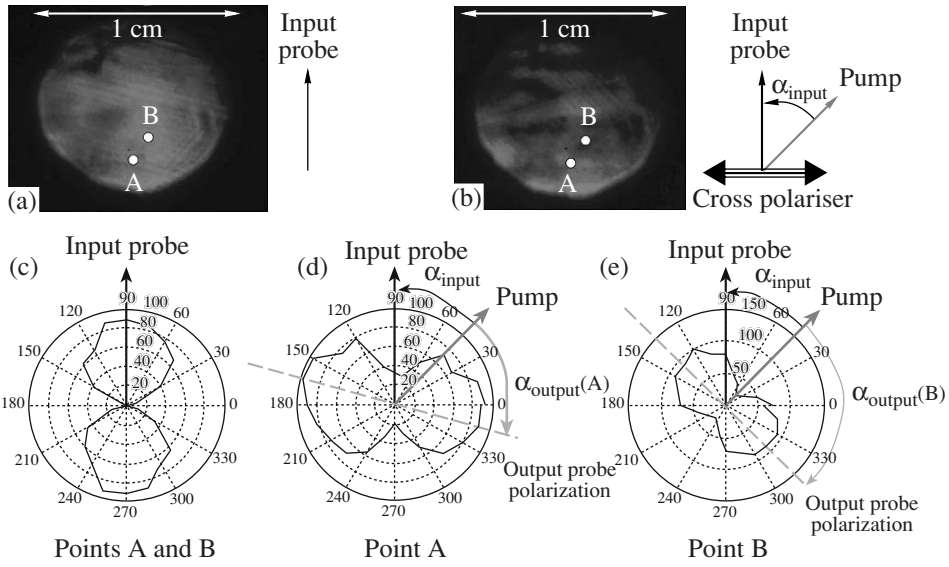

Fig. 7. Inhomogeneous distribution of the filament-induced ultrafast birefringence resulting from the profile of the pump intensity. (a) Intensity profile of the homogeneously polarized input probe beam. (c) Both points A and B exhibit the same linear polarization. (b) Output probe beam intensity distribution measured through a polarizer orthogonal to the incident probe polarization ($\alpha_{input}(A) = \alpha_{input}(B) = -45°$ with respect to the pump polarization). The inhomogeneous pump intensity profile is transferred to the pump polarization. As a result, the angular polarization distributions at points A and B are different: $\alpha_{output}(A) = +60°$ (d) and $\alpha_{output}(B) = +90°$ (e), respectively [21].

As can be seen on Fig. 6b, our simulations show that higher pressures (i.e., higher n_2^{SPM} values) result in longer filaments with lower intensity clamping [24, 25]. These opposite effects roughly compensate each other when calculating the integral $\int I^{filament}(z)dz$, so that the dephasing $\Delta\varphi_{XPM}^{probe} = 2\pi n_2^{XPM}\int I^{filament}(z)dz/\lambda_{probe}$ varies like n_2^{XPM}, i.e., with a linear dependence with Argon pressure.

As the filament-induced dephasing depends monotonically on pressure, any $\Delta\varphi_{XPM}^{probe}$ value may be generated by choosing an adequate Argon pressure. For example, an interpolation of the experimental data presented in Fig. 6 suggests that an equivalent "λ/4 plate" can be generated for 1.7 ± 0.1 bar.

6. TRANSVERSE DISTRIBUTION OF INDUCED BIREFRINGENCE

The filament-induced dephasing $\Delta\varphi_{XPM}^{probe}$ given in Eq. (5) results from the integration of the filament intensity over its whole copropagation with the probe beam. Since the intensity profile of the filamenting beam is far from homogeneous, $\Delta\varphi_{XPM}^{probe}$ also exhibits a transverse distribution, which will be transfered onto the probe polarization profile, as displayed in Fig. 7 for a 3 bar Argon pressure. In order to illustrate such modification of the probe polarization distribution, we selected two distinct points of the probe transverse profile, noted A and B on Fig. 7: while they have the same linear polarization before the interaction with the filament (Fig. 7c), they bear different elliptical polarizations after copropagation (Figs. 7d, 7e). Their contrast ration are equivalent around 67%, but their main axes have different orientations with respect to the direction of the filamenting pulse polarization ($\alpha_{output}(A) = +60°$ and $\alpha_{output}(B) = +90°$, respectively, while $\alpha_{input}(A) = \alpha_{input}(B) = \alpha_{input} = -45°$). This transverse distribution of the induced birefringence bears valuable information about the transverse intensity distribution in the filament, although this information is integrated over the whole co-propagation distance. Further investigations are to be performed to quantitatively describe the complete filament-induced birefringence pattern distribution.

7. CONCLUSIONS

In conclusion, we have demonstrated that laser-generated self-guided filaments can induce significant birefringence in near-atmospheric pressure gases. An angle of 45° between the filament and the probe polarizations allows the realization of Kerr-gates, with an unprecedented switching time ultimately limited by the duration of the filamenting pulse. An optical ultrafast switch could even be initiated remotely by self-guided filaments in the atmosphere [6, 26–28], even in perturbed conditions [29–31], opening new perspectives for

remote optical ultrafast data transmission and processing, e.g., remote ultrafast optical logical gates.

Moreover, we have shown that the transverse probe polarization distribution, which originates from the transverse intensity profile of the filament, is transferred onto the transverse probe beam polarization distribution, as a result of the transverse distribution of the Kerr-induced birefringence. The resulting polarization map can be used as a diagnostics to analyze the filament internal structure and intensity profile.

ACKNOWLEDGMENTS

This work was supported by the Swiss NSF (contract 200021-111688 and R'equip program), and the Swiss SER in the framework of COST P18 action C06.0114, as well as the Boninchi and Schmideiny foundations.

REFERENCES

1. A. Braun, G. Korn, X. Liu, et al., Opt. Lett. **20**, 73 (1995).
2. S. L. Chin, S. A. Hosseini, W. Liu, et al., Can. J. Phys. **83**, 863 (2005).
3. L. Bergé, S. Skupin, R. Nuter, et al., Rep. Prog. Phys. **70**, 1633 (2007).
4. A. Couairon, and A. Mysyrowicz, Phys. Rep. **441**, 47 (2007).
5. J. Kasparian, and J.-P. Wolf, Opt. Express **16**, 466 (2008).
6. J. Kasparian, M. Rodriguez, G. Méjean, et al., Science **301**, 61 (2003).
7. J. Kasparian, R. Ackermann, Y.-B. André, et al., Opt Express **16**, 5757 (2008).
8. C. P. Hauri, W. Komelis, F. W. Helbing, et al., Appl. Phys. A **79**, 673 (2004).
9. S. A. Trushin, K. Kosma, W. Fuss, et al., Opt. Lett. **32**, 2432 (2007).
10. P. Béjot, J. Kasparian, and J.-P. Wolf, Opt. Express **16**, 14115 (2008).
11. S. Petit, A. Talebpour, A. Proulx, et al., Opt. Commun. **175**, 323 (2000).
12. G. Fibich and B. Ilan, Phys. Rev. E **67**, 036622 (2003).
13. H. Yang, J. Zhang, Q. J. Zhang, et al., Opt. Lett. **30**, 534 (2005).
14. M. Kolesik, J. V. Moloney, and E. M. Wright, Phys. Rev. E **64**, 046607 (2001).
15. S. Tzortzakis, B. Prade, M. Franco, et al., Opt Commun. **181**, 123 (2000).
16. J. P. Geindre, P. Audebert, A. Rousse, et al., Opt. Lett. **19**, 1997 (1994).
17. Y. H. Chen, S. Varma, I. Alexeev, et al., Opt. Express **15**, 7458 (2007).
18. P. Béjot, Y. Petit, L. Bonacina, et al., Opt Express **16**, 14115 (2008).
19. M. Mlejnek, E. M. Wright, and J. V. Moloney, Phys. Rev. E **58**, 4903 (1998).
20. P. Béjot, C. Bonnet, V. Boutou, et al., Opt. Express **15**, 13295 (2007).
21. Y. Petit, P. Béjot, L. Bonacina, et al., in *Proc. of the 17th Intern. Laser Physics Workshop LPHYS'08, Trondheim, Norway, 30 June–4 July, 2008*.
22. G. P. Agrawal, *Nonlinear Fiber Optics* (Academic, San Diego, 2001).
23. J. Kasparian, R. Sauerbrey, and S. L. Chin, Appl. Phys. A **71**, 877 (2000).
24. P. Sprangle, E. Esarey, and B. Hafizi, Phys. Rev. E **56**, 5894 (1997).
25. A. Becker, N. Aközbek, K. Vijayalakshmi, et al., Appl. Phys. A **73**, 287 (2001).
26. B. La Fontaine, F. Vidal, Z. Jiang, et al., Phys. Plasmas **6**, 1615 (1999).
27. M. Rodriguez, R. Bourayou, G. Méjean, et al., Phys. Rev. E **69**, 036607 (2004).
28. G. Méchain, A. Couairon, Y.-B. André, et al., Appl. Phys. A **79**, 379 (2004).
29. G. Méjean, J. Kasparian, J. Yu, et al., Phys. Rev. E **72**, 026611 (2005).
30. G. Méchain, G. Méjean, R. Ackermann, et al., Appl. Phys. A **80**, 785–789 (2005).
31. R. Salamé, N. Lascoux, E. Salmon, et al., Appl. Phys. Lett. **91**, 171106 (2007).